Comparative Biochemistry and Physiology, Part B 263 (2023) 110783

Contents lists available at ScienceDirect

Comparative Biochemistry and Physiology, Part B

journal homepage: www.elsevier.com/locate/cbpb

Characterization of larval shell formation and *CgPOU2F1*, *CgSox5,* and *CgPax6* gene expression during shell morphogenesis in *Crassostrea gigas*

Yue Min [a], Qi Li [a,b,*], Hong Yu [a]

[a] Key Laboratory of Mariculture (Ocean University of China), Ministry of Education, and College of Fisheries, Ocean University of China, Qingdao 266003, China
[b] Laboratory for Marine Fisheries Science and Food Production Processes, Qingdao National Laboratory for Marine Science and Technology, Qingdao 266237, China

ARTICLE INFO

Edited by Chris Moyes

Keywords:
Mollusks
Shell field
Shell formation
Larvae

ABSTRACT

Shell formation is a dynamic process involving organic matrix secretion and calcification. In this study, we characterized shell morphogenesis during larval development in *Crassostrea gigas.* Using scanning electron microscopy (SEM) and fluorescence staining, we demonstrated that shell field, the first morphologically distinguishable shell-forming tissue, became visible soon after enlargement of the blastopore at the anterior end of the trochophore. Shell organic matrix namely protein polysaccharides and calcified structure appeared as a slit at the dorsal side of the embryo. The early shell field began to extend along the dorsal side of the trochophore larvae, and became a saddle shaped shell field that gave rise to the prodissoconch I embryonic shell in the early D-shaped larvae. Subsequently, prodissoconch II shell was formed in the late D-shaped larvae with a characteristic appearance of growth lines. To identify gene expression markers for studying shell formation, we isolated three potential larval shell formation genes *CgPOU2F1*, *CgSox5*, and *CgPax6* and analyzed their expression during shell morphogenesis. The three potential shell formation genes possessed a similar pattern of expression. Their expression was detected in the shell gland and shell field regions in early D-shaped larvae, hereafter, their expression was detected at the larval mantle edge in the calcified shell stages. Together, these studies provide knowledge of shell morphogenesis in pacific oyster and molecular markers for studying the molecular regulation of biomineralization and shell formation.

1. Introduction

Biomineralization by living organisms is a dynamic biological process to generate mineralized tissues with diverse biological functions including tissue support, protection, mineral storage, shelter against predation, and magnetic field perception (Song et al., 2019). In metazoan, the diverse mineralized exoskeletons contribute, in part, to the rapid establishment of shell-bearing mollusks during evolution. Molluscan shells are organo-mineral complex made up of approximately 95% calcium carbonate ($CaCO_3$) and 1%–5% organic components (Song et al., 2019). The organic matrix is the major source of macromolecules including glycoproteins, chitin, and acidic polysaccharides that play important roles in crystal nucleation and growth (Marin et al., 2005; Addadi et al., 2006; Suzuki et al., 2009). Shell matrix proteins (SMPs) have been identified from a variety of mollusk species using genomic, transcriptomic, and proteomic approaches in *Crassostrea gigas* (Marie et al., 2011; Zhang et al., 2012), *Hyriopsis cumingii* (Berland et al., 2013), *Mytilus edulis* (Liao et al., 2015), *Haliotis asinine* (Marie et al., 2010) and *Lottia gigantea* (Marie et al., 2013). These studies revealed a complexity of macromolecules and structural diversity of SMPs between species (Jackson et al., 2010).

Shell formation starts early in larval development in bivalves. Bivalves form two types of shells during larval development, namely prodissoconch I and II shell (Zhao et al., 2018). They are generated by distinct tissues at different developmental stages. The embryonic shell, prodissoconch I, is established by organic components secreted by the ectodermal cells (shell gland) in the dorsal region of trochophore larvae (Aranda-Burgos et al., 2014). Subsequently, the larval shell, prodissoconch II, is generated by the veliger larval mantle (Freeman and Lundelius, 1999; Che et al., 2001). Adult shell begins to form after metamorphosis using organic components secreted from mantle (Zhao et al., 2018). Evidently, shell components displayed extensive dynamic changes during shell morphogenesis as reflected by changes in calcium carbonate crystal polymorphisms and shell layer structures (Rose and Baker, 1994). Prodissoconch I is mainly composed of amorphous calcium carbonate (ACC) found in shells during trochophore larval stage,

* Corresponding author at: Key Laboratory of Mariculture, Ministry of Education, Ocean University of China, Qingdao 266003, China.
E-mail address: qili66@ouc.edu.cn (Q. Li).

https://doi.org/10.1016/j.cbpb.2022.110783
Received 14 May 2022; Received in revised form 28 July 2022; Accepted 29 July 2022
Available online 1 August 2022

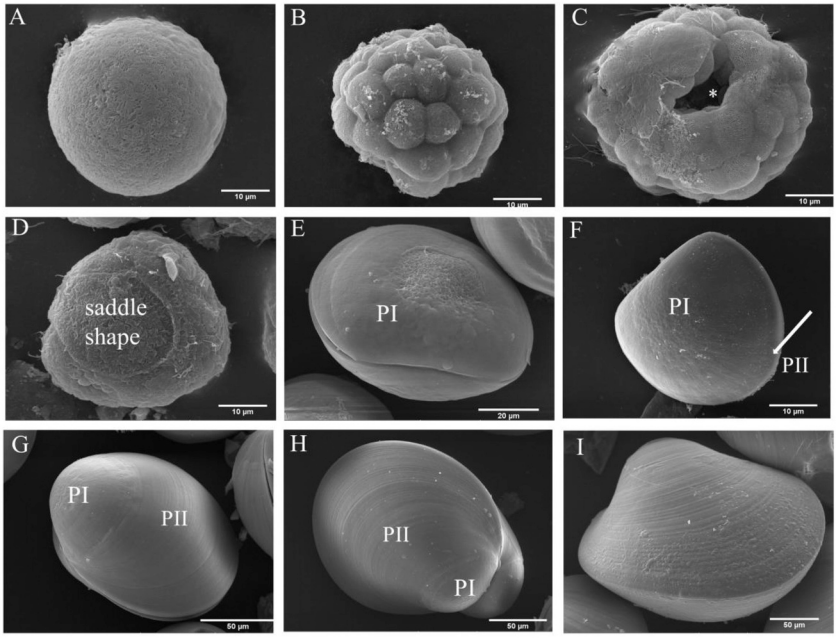

Fig. 1. SEM analysis of larval development in *C. gigas*. A: fertilized egg; B: multicellular larvae (2-3hpf); C: gastrula larvae (8hpf), the shell gland begins to be seen as a slit (asterisk); D: trochophore (10hpf); E: D-shaped larvae (12hpf); F: D-shaped larvae (2dpf); G: Umbol larvae (10dpf); H: eyespot larvae (28dpf).

whereas prodissoconch II, which consists of aragonite and calcite, forms at the veliger larval stages (Miyazaki et al., 2010; Lee et al., 2006). During early veliger larval stage, the aragonite makes up of approximately 92% (Lee et al., 2006). The adult shell of marine bivalves, also known as dissoconch shell, is composed of calcite and aragonite (Fang et al., 2011).

Mollusks, such as *Crassostrea gigas,* are marine calcifiers of economically importance. *C. gigas* is one of the most important species in aquaculture around the world. In addition, it is also a useful model for developmental studies owing to its mosaic pattern of early embryos and interesting life cycle from the free-swimming state to the immobile sessile. Shell formation is an important event during the larval developmental process. Several studies have been conducted on *C. gigas* larvae to identify novel shell formation genes. Several genes, such as SoxC, gata2/3, engrailed, and tyr1, have been identified that showed expression in larval mantle of *C. gigas* (Huan et al., 2013; Liu et al., 2015; Liu et al., 2017).

In the present study, SEM and larval shell staining were performed to observe the dynamic morphological changes during shell formation in *C. gigas*. Additionally, several potential shell formation genes were identified, and their expression profiles were determined during shell biomineralization and formation. Whole-mount in situ hybridization revealed that these potential shell formation genes were expressed in the shell field, thus providing molecular markers for future studying the molecular regulation of biomineralization and shell formation.

2. Materials and methods

2.1. Sample collection

C. gigas embryos and larvae were collected from Laizhou, Shangdong, China at the following developmental stages: fertilized egg (1 h-post-fertilization [hpf]), multicell (2–3 hpf), blastula (5hpf), gastrula (8hpf), trochophore (11hpf), early D-shaped larvae (12hpf), D-shaped larvae (2 days post-fertilization [dpf]), early Umbo larvae (10dpf), late Umbo larvae (16 dpf) and eyed larvae stages (28dpf). Samples for RNA extraction were stored in RNA-store solution (Dongsheng Biotech, China) at −20 °C. For scanning electron microscopy (SEM), larvae were fixed in 2.5% glutaraldehyde in 0.1 M phosphate buffer solution (PBS). For whole-mount in situ hybridization (WISH), specimens were fixed in 4% paraformaldehyde at 4 °C overnight. D-shaped larvae, Umbo larvae, and eyed larvae were anesthetized with the gradual addition of 7.5% $MgCl_2$ solution to the seawater before they were collected and fixed. After fixation overnight, samples were washed and dehydrated with 100% methanol and stored in 100% methanol at −20 °C until use.

2.2. Total RNA extraction and synthesis of cDNA

TRIzol reagent (Invitrogen, USA) was used to extract total RNA from the samples according to the manufacturer's instructions. The quality and concentration of RNAs were determined by Nanodrop 2000 (Thermo, USA) and analyzed in a 1.5% agarose gel electrophoresis. The first-strand cDNA was synthesized using the PrimeScript™ 1st strand cDNA Synthesis kit (Takara, Japan).

2.3. Cloning of the full-length cDNA sequences

The cDNA coding sequences of *CgPOU2F1*, *CgSox5,* and *CgPax6* were isolated by PCR based on the sequence information from the National Centre for Biotechnology Information (NCBI, https://www.ncbi.nlm.nih.gov; Accession: POU2F1: LOC105318365; Sox5: LOC105326856; Pax6: LOC105332393). Specific primers were designed by the Primer Premier 5.0 software (Premier Biosoft International, Palo Alto, CA) in Table S1. The PCR was performed using Phanta Max super-Fidelity DNA polymerase (Vazyme, China) using the following condition: predenaturation at 95 °C 3 min; 95 °C for 15 s, Tm for 15 s, 72 °C for 30–60s/kb, 35 cycles; 72 °C for 5 min. The PCR products were purified and cloned into pMD-19 T vector (Takara, Japan). The sequences were determined by Sanger sequencing method.

2.4. Sequence and phylogenetic analyses

The amino acid sequences of *CgPOU2F1*, *CgSox5*, and *CgPax6* were analyzed for homology using the BLAST programs hosted by the NCBI. Conserved domains prediction was performed using NCBI conserved domain search (CD-Search). The functional domains were predicted using SMART software (http://smart.embl-heidelberg.de/). Multiple sequences alignments were conducted using DNAMAN version 6.0

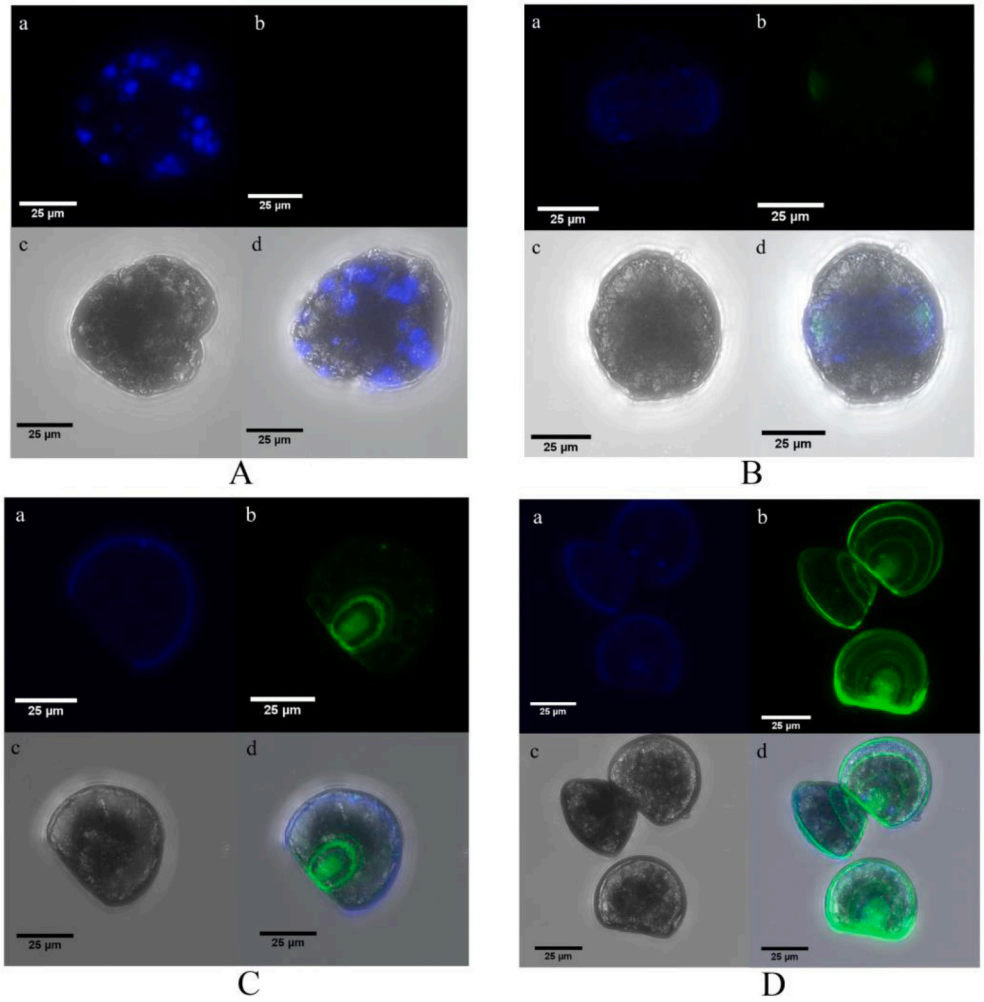

Fig. 2. Confocal images showing the time course of shell formation in *C. gigas* from gastrula (6hpf) to the D-shaped stage (24hpf). a: calcofluor fluorescent signal (blue); b: calcein fluorescence signal (green); c: brightfield image of the embryo; d: merged calcofluor, calcein, and brightfield images. A, B, C, D represent 6hpf, 10hpf, 12hpf, and 24hpf respectively. (For interpretation of the references to color in this figure legend, the reader is referred to the web version of this article.)

(Lynnon Biosoft, USA) program, and the phylogenetic tree was constructed using the neighbor-joining (NJ) method in MEGA7 with 1000 bootstrap replications. The accession numbers of genes included in multiple sequence alignment and phylogenetic analysis were shown in Table S2.

2.5. Expression analysis by real-time quantitative PCR

To characterize the expression of *CgPOU2F1*, *CgSox5* and *CgPax6* during *C. gigas* embryonic, we quantified their transcript levels at different developmental stages by qPCR. The qPCR was performed using the QuantiNova SYBR Green PCR kit (Qiagen, Germany) on a Lightcycler® 480 real-time PCR instrument (Roche, Switzerland). The specific primers were designed using primer premier 5.0 software (Premier Biosoft International, Palo Alto, CA) and listed in Table S1. Their specificity was confirmed by conventional PCR and melting curve analysis. The arf1, ef1α and gapdh were used as internal controls (Huan et al., 2016). The relative expression was calculated by the $2^{-\Delta\Delta CT}$ method. All the data and significant differences were analyzed using GraphPad Prism 8.0 by one-way ANOVA followed by multiple comparisons. Differences were considered statistically significant at $P < 0.05$.

2.6. Whole-mount in situ hybridization

Whole-mount in situ hybridization (WISH) was used to analyze the pattern of gene expression at various developmental stages. The gene-specific primers for sense and antisense probes were shown in Table S1. For sense probe synthesis, the forward primers were tagged with a T7 primer sequence (GATCACTAATACGACTCACTATAGGG). In contrast, for antisense probes, the reverse primers were tagged with the T7 primer sequence. Together with respective reverse and forward primers without the T7 primer sequence, digoxigenin-labeled sense and antisense probes were synthesized using the DIG-RNA labeling kit (Roche, Switzerland). WISH was conducted using the protocol with some modifications (Hohagen et al., 2015). Briefly, after washing with PBST (PBS, 0.1% Tween-20), embryos were treated with protease K of different concentrations depending on the embryonic stages (Solarbio, China) for 30 min at 37 °C. For D-shaped larvae, Umbo larvae, and eyed larvae, they were treated with 0.5 M EDTA for 0.5, 6 and 7 h respectively before protease K treatment. Prehybridization was carried out in hybridization buffer (20× SSC, 50% Formamide deionized, 500 μg/ml tRNA, 50 μg/ml heparin, 0.1% Tween-20, 9.2 mM citric acid) at 65 °C for 5-6 h. Then hybridized with 500 ng/ml antisense or sense probe overnight at 65 °C. After removal of the hybridization solution, all samples were rinsed with low salt washing buffer and then blocking buffer. The embryos were incubated with anti-digoxigenin-AP Fab fragments (Roche, Switzerland) diluted 1:5000 at 4 °C overnight. Color reaction was performed in 2% NBT/BCIP solution (Roche, Switzerland) for 1-3 h at room temperature in the dark. Samples were photographed using an Olympus BX53 microscope equipped with a DP80 camera

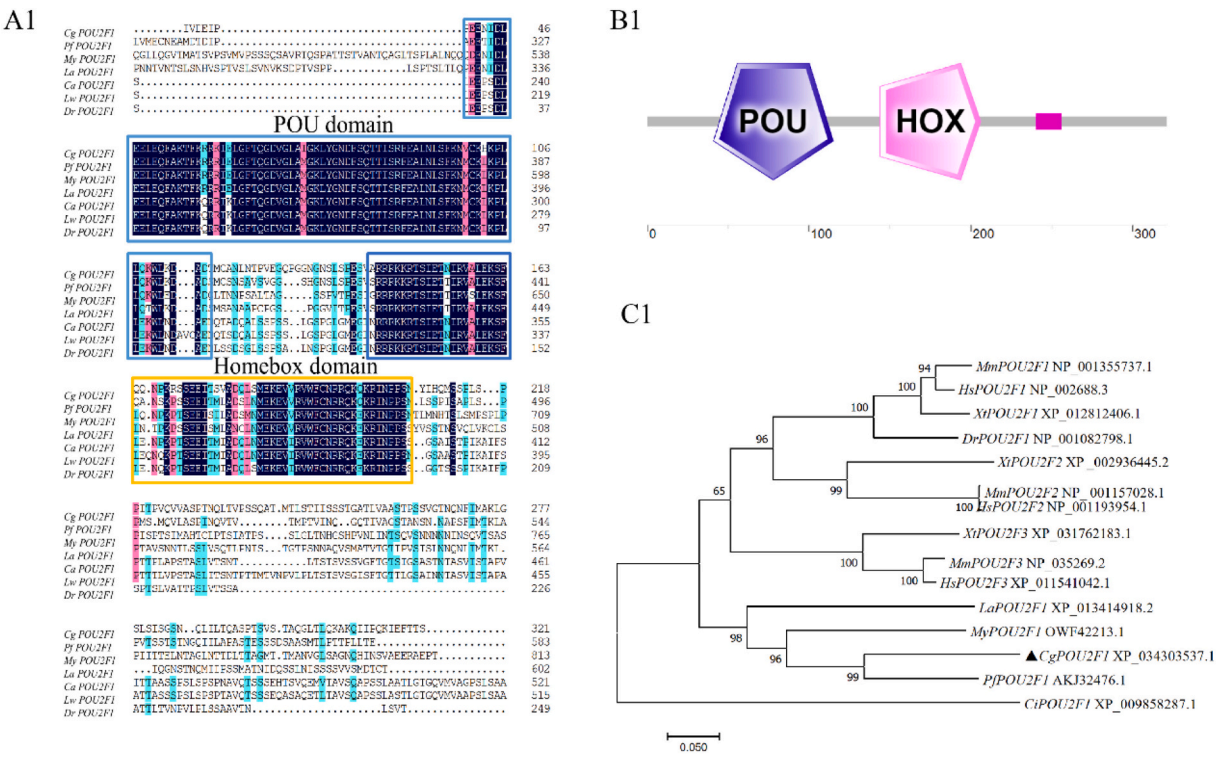

Fig. 3. Sequence alignment and phylogenetic analysis of *POU2F1*. A: The alignment of the deduced CgPOU2F1 amino acid sequence with homologous sequences in other species. B: The predicted structures of the POU2F1 protein in *C. gigas*. C: The phylogenetic analysis of the CgPOU2F1 protein.

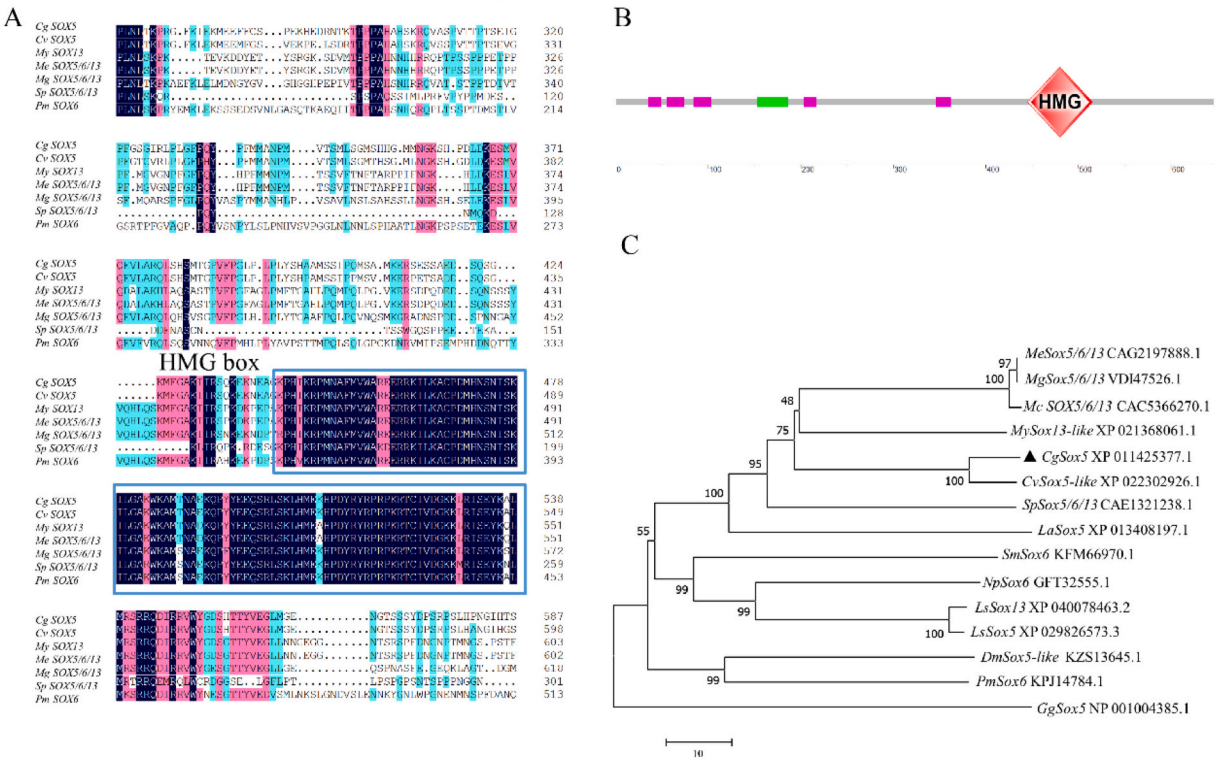

Fig. 4. Sequence alignment and phylogenetic analysis of *Sox5*. A: The alignment of the deduced CgSox5 amino acid sequence with homologous sequences in other species. B: The predicted structures of the Sox5 protein in *C. gigas*. C: The phylogenetic analysis of the CgSox5 protein.

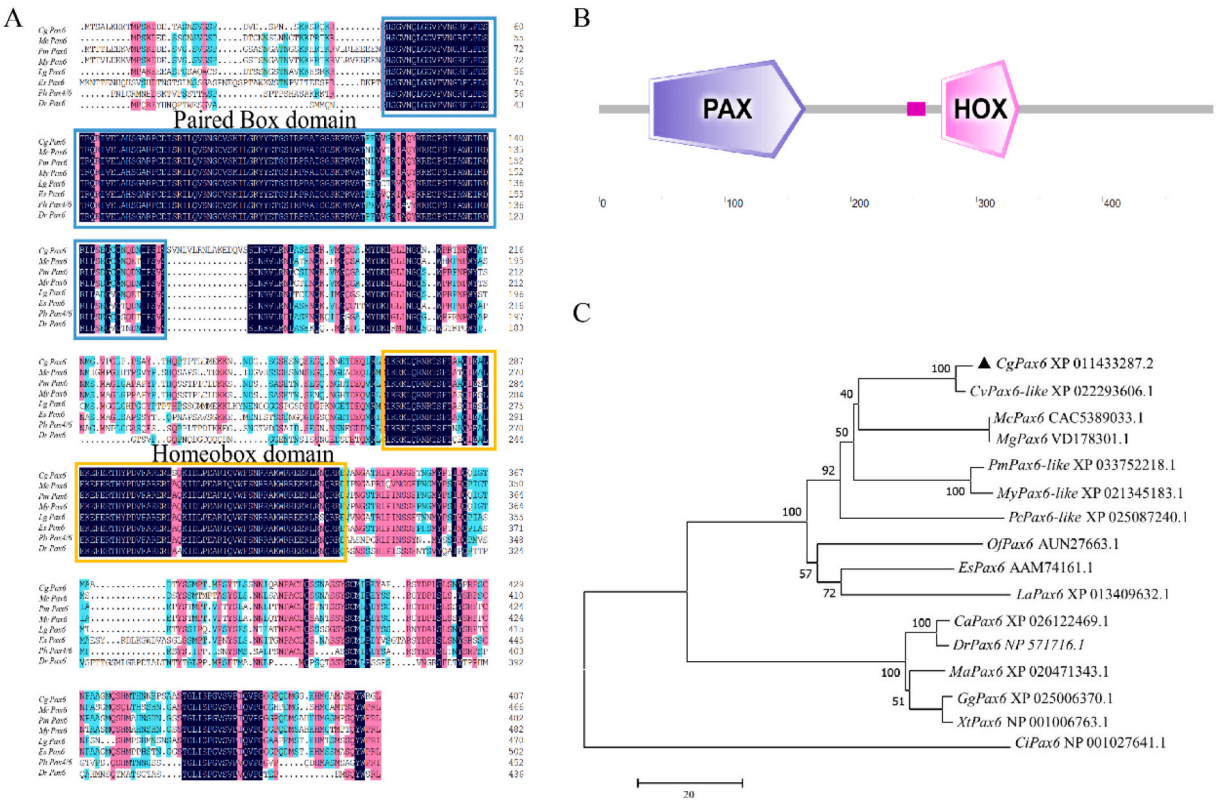

Fig. 5. Sequence alignment and phylogenetic analysis of *Pax6*. A: The alignment of the deduced CgPax6 amino acid sequence with homologous sequences in other species s. B: The predicted structures of the Pax6 protein in *C. gigas*. C: The phylogenetic analysis of the CgPax6 protein.

(Olympus, Japan).

2.7. SEM analysis of shell biogenesis

SEM was performed to examine larval shell morphogenesis. Briefly, samples were fixed in 2.5% glutaraldehyde in 0.1 M phosphate buffer solution (PBS) and then refixed in 1% osmic acid. After fixation, the samples were washed in PBS and dehydration was done using a graduated series of ethanol. Subsequently, samples were dehydrated using chloroform and let them dry in a sealed glass Petri dish. Once dried, samples were coated with gold and scanned using the VEGA3 TESCAN scanning electron microscope.

2.8. Calcein and calcofluor staining

Calcein and calcofluor white staining were performed to visualize calcified structure and polysaccharides in shell field, respectively (Kapsenberg et al., 2018; Miglioli et al., 2019). These two fluorescent dyes were added at different times to the live samples. Calcein was added into filtered seawater used to incubate fertilized eggs, while calcofluor (Fluorescent Brightener 28) was added to seawater containing the embryo and larvae five minutes before sampling. Upon sampling time (before D-shaped larvae), larvae were fixed with 4% paraformaldehyde (PFA) in filtered seawater, and then were immediately washed three times in filtered seawater to remove excess dyes. After washing, the samples were imaged by the Lecia TCS SP8 (Lecia, France).

3. Results

3.1. SEM analysis of shell morphogenesis in C. gigas

The embryogenesis and process of shell formation were analyzed using SEM during early embryonic and larval development. After fertilization, the single cell embryo went through a cleavage process to become a morula of approximately 64 cells around 4–5 hpf. By 8hpf, shell gland appeared as a slit at the dorsal side of the gastrula stage embryo (Fig. 1-C). The early shell field began to extend along the dorsal side of the trochophore larvae, and became a saddle shaped shell field in early D-shaped larvae around 12hpf (Fig. 1-D). The saddle shaped shell field further expanded to cover the entire larvae and gave rise to the prodissoconch I larval shell (Fig. 1-E), although the shell surface was not well established (Fig. 1-E). Subsequently, prodissoconch II shell was formed in the late D-shaped larvae with a characteristic appearance of growth lines (Fig. 1-F). The growth lines were more apparent in larvae of Umbo and eyespot stages (Fig. 1G-I).

3.2. Confocal analysis of shell matrix deposition and calcification during shell morphogenesis

Organic shell matrix and calcified structures were analyzed in developing embryos from gastrula to D-shaped stage (6, 10, 12 h, and 24 h) by double staining using calcofluor and calcein that bind to polysaccharides and calcium, respectively. As shown in Fig. 2, gastrula larvae started to secrete organic matrix at 6hpf. A clear calcofluor signal (blue) was visible around the outline of the gastrula larvae, whereas the calcein signal was not detectable. At 10hpf, signals from calcein staining became visible in a saddle-shaped area corresponding to the early shell field (Fig. 2-B), which is consistent with the SEM results (Fig. 1-D). The larval shell began to take shape as calcein signal gradually appeared at the shell gland of the larvae. At 12hpf, the shell field was expanded and calcein fluorescent signal was intense at the center of the forming shell. By 24hpf, the calcified shell covered the entire larvae, with clear growth lines revealed by calcein staining (Fig. 2-D). The Umbo larvae and eyespot larvae were also stained by calcein and calcofluor (not provided), but the calcein signal was not clear, likely because fixed larvae did not bind well to calcein or calcofluor.

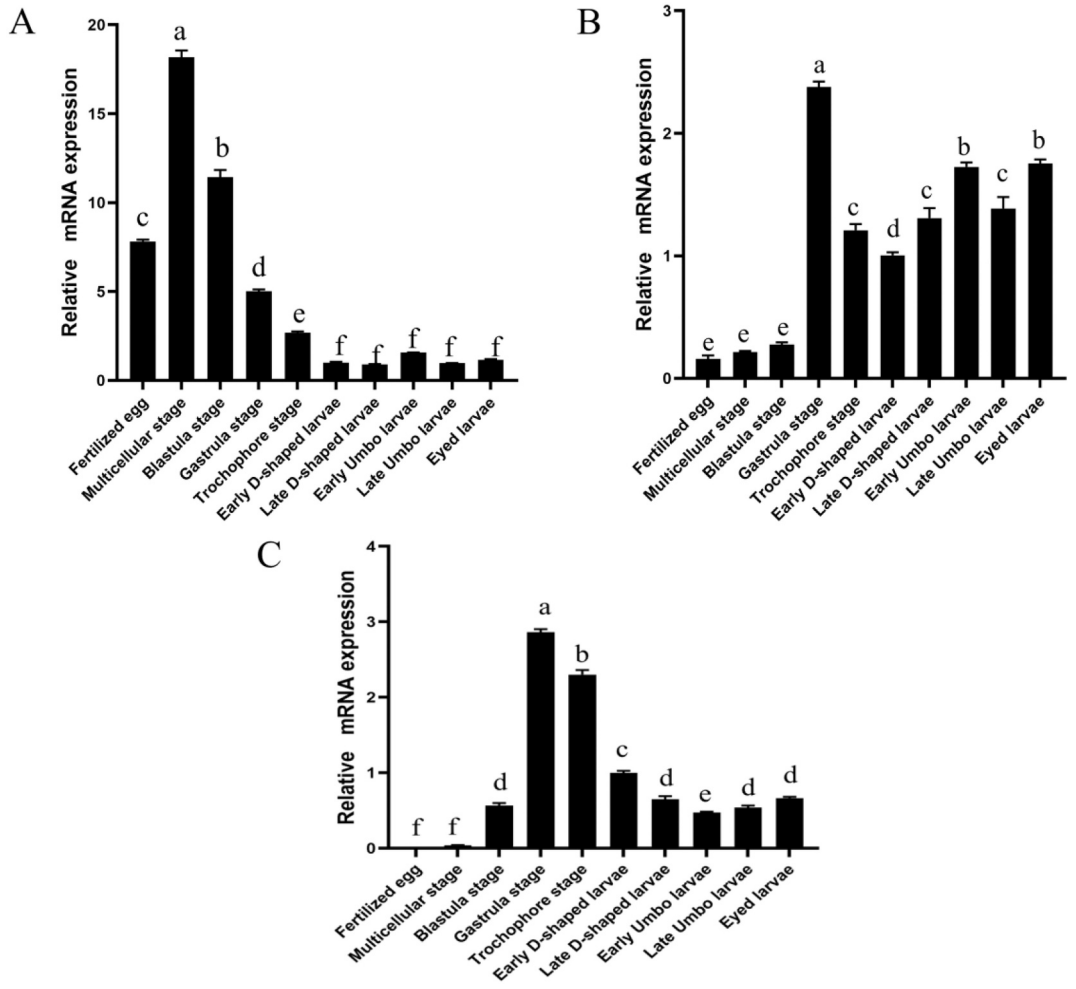

Fig. 6. The spatial pattern of mRNA expression at various embryonic and larval developmental stages. A, B, and C represent expression patterns of *CgPOU2F1*, *CgSox5*, and *CgPax6* in different developmental stages of *C. gigas*.

3.3. Gene cloning and sequence analysis

CgPOU2F1, *CgSox5*, and *CgPax6* genes were identified through genomic data (PRJNA629593). Their CDNAs were cloned and sequenced. ORFs of 966 bp, 1941 bp, and 1464 bp were identified in *CgPOU2F1*, *CgSox5*, and *CgPax6* that encode a 321, 647 and a 488-amino acid (AA) peptide, respectively. Amino acid sequence alignments of *CgPOU2F1*, *CgSox5*, and *CgPax6* from *C. gigas* were performed and shown in Figs. 3, 4, 5. The *CgPOU2F1* showed 19.48% identity to the *Pinctada fucata POU2F1*, 15.48% with *POU2F1* of *Mizuhopecten yessoensis*. The *CgSox5* shared 78.47% identity with *Crassostrea virginica* SRY-box13, and 47.33% with *M. yessoensis* SRY-box13. The *CgPax6* shared the highest (70.37%) identity with *Pecten maximus*, and 69.63% with *M. yessoensis*. Further conserved domain analysis revealed that *CgPOU2F1* possessed a POU domain and a Homeobox domain. As for the *CgSox5* and *CgPax6*, an HMG box, Paired Box domain, and Homeobox domain were identified, respectively.

3.4. Phylogenetic analysis of CgPOU2F1, CgSox5, and CgPax6

Phylogenetic analysis was performed to investigate the relationship between *CgPOU2F1*, *CgSox5*, and *CgPax6* and other members of their respective gene families. The POU2F1 and other family members formed three separate groups in vertebrates and invertebrates. Pacific oyster POU2F1, together with POU2F1 from other mollusca formed a major distinct group from vertebrate homologs (Fig. 3-C). The *CgSox5* clustered with *Sox5/6/13* from other mollusca and brachiopoda, then clustered with arthropoda homologs (Fig. 4-C). The *CgPax6* clustered with other Pax6 in other bivalves to form a major distinct group (Fig. 5-C).

3.5. Temporal expression patterns of CgPOU2F1, CgSox5, and CgPax6 during larval development

The expression patterns of *CgPOU2F1*, *CgSox5*, and *CgPax6* were analyzed at different developmental stages. The data showed that all three genes were mostly expressed in all developmental stages analyzed. *CgPOU2F1* was strongly expressed at the multicellular stage around 3-4hpf. Its expression level decreased dramatically during development (Fig. 6-A). The expression profile of *CgPax6* were similar to the *CgSox5* (Fig. 6-C). *CgPax6* was rarely expressed in fertilized eggs and multicellular stage, while its expression increased rapidly reached the maximum at the gastrula stage (Fig. 6-C). *CgPax6* expression decreased dramatically from the trochophore stage to the eyed larval stage. The expression profile of *CgSox5* were extremely different from *CgPOU2F1* and *CgPax6*. High levels of *CgSox5* expression was detected at the gastrula stage (Fig. 6-B) and maintained a high level with slight fluctuations.

3.6. Spatial pattern of CgPOU2F1, CgSox5, and CgPax6 expression during larval development

The temporospatial patterns of *CgPOU2F1, CgSox5, and CgPax6*

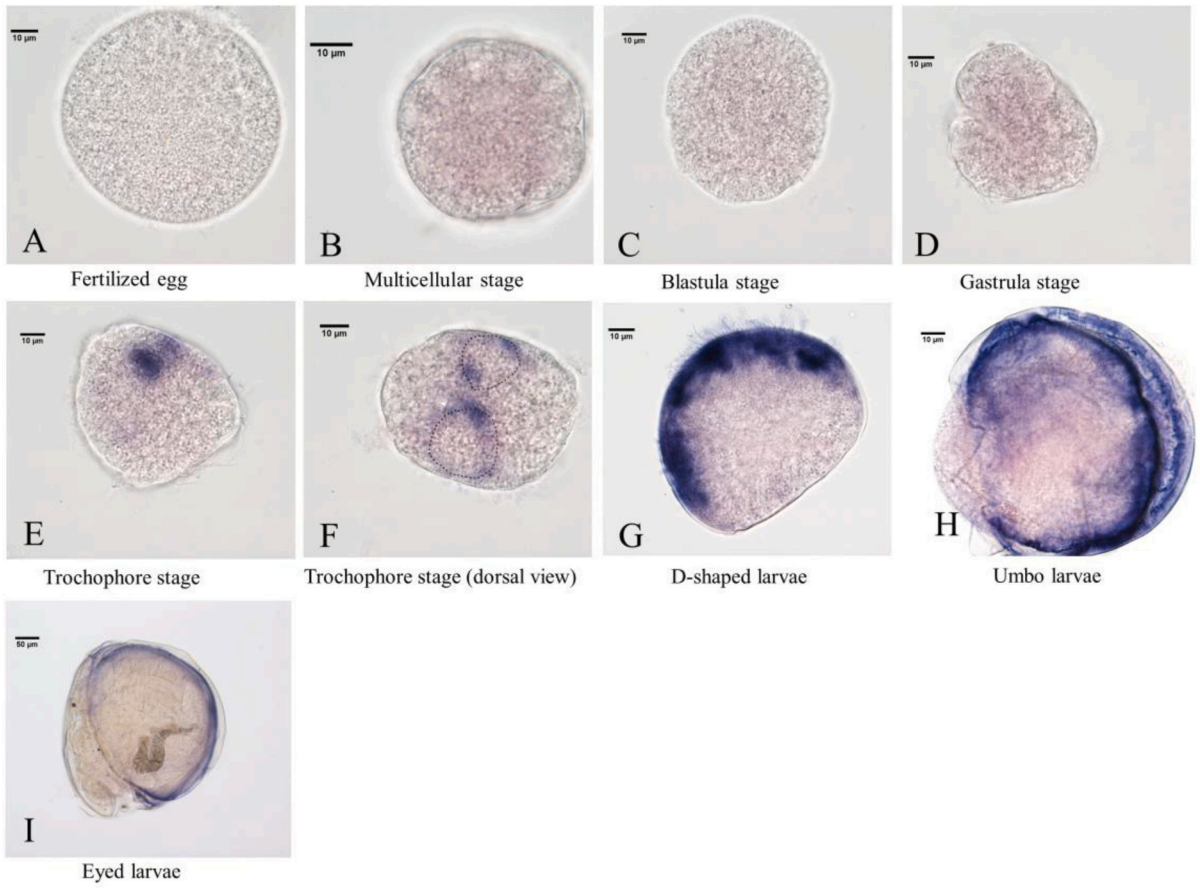

Fig. 7. The spatial pattern of *CgPOU2F1* expression in embryos and larvae at different developmental stages.

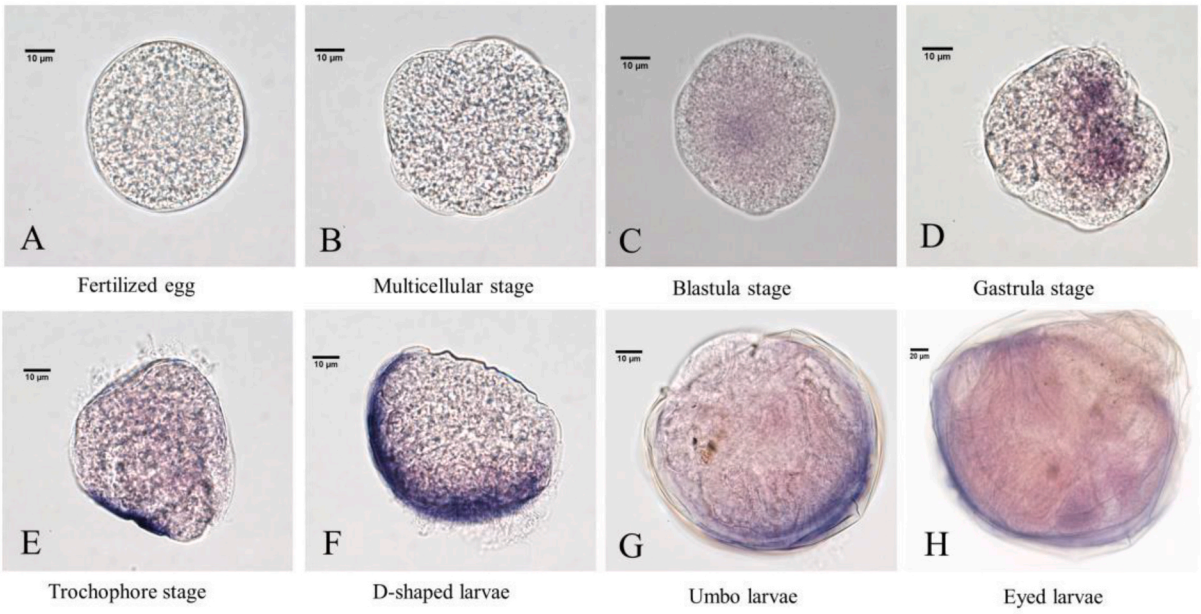

Fig. 8. The spatial pattern of C*gSox5* expression in embryos and larvae at different developmental stages.

expression were determined from fertilized egg to the eyespot stage using WMISH. A similar pattern of expression was detected for the three potential shell formation genes. Positive signal of *CgPOU2F1* was first detected in the saddle-shaped shell field area at the trochophore stage (Fig. 7-E, 7-F). Later, *CgPOU2F1* expression appeared in larval mantle edge of later developmental stages (Fig. 7). As for *CgSox5*, a positive signal was first detected in the shell gland of gastrula stage embryos (Fig. 8-D), and later appeared in the larval mantle edge. The expression patterns of *CgPax6* were similar to *CgPOU2F1*, with initial detection in shell field of the trochophore stage (Fig. 9-E), and then appeared at the

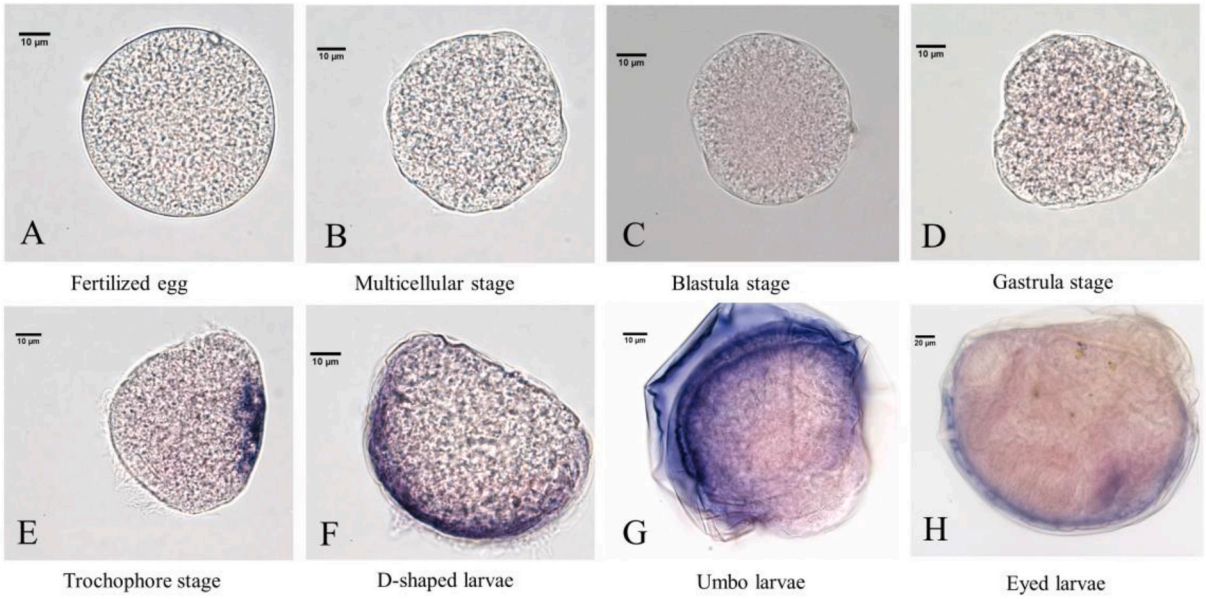

Fig. 9. The spatial pattern of *CgPax6* expression in embryos and larvae at different developmental stages.

edge of larval mantle in calcified shell stages. The negative control of three genes were shown in the Figs. S1–S3.

4. Discussion

During development, larval shell formation is driven by shell matrix, which plays a crucial role in $CaCO_3$ deposition and shell growth (Miglioli et al., 2019). In this study, we analyzed the secretion of organic matrix and $CaCO_3$ deposition by the double staining using calcofluor and calcein. We showed that the calcification area was proceeded by an expansion of the organic matrix. In addition, the organic layer is in a position to protect initial shell structures from dissolution during adverse environmental conditions such as lowered saturation state for aragonite (Ramesh et al., 2018). Furthermore, the $CaCO_3$ deposition becomes more vividly during shell growth. Together, these data clearly indicate a close interaction between shell organic matrix and calcification. Organic matrix may provide raw material for calcification to take place in the early stages of shell formation.

Currently, the mechanism underlying molluscan larval shell formation is largely unknown. The dynamic developmental events are regulated by gene regulatory networks (GRNs) to precisely regulate the spatial and temporal expression of downstream "effector" genes involved in various steps of tissue patterning and cell differentiation (Exelby et al., 2021). Several regulatory factors have been implicated in shell-field development in molluscan. These include T-box transcription factor Brachyury, homeobox transcription factor Distal-less, homeodomain transcription factors of Engrailed and various Hox genes as well as one morphogenetic proteins BMP2 and BMP4 (Jackson and Degnan, 2016). In our previous study, *CgPOU2F1*, *CgSox5*, and *CgPax6* were three potential transcription factors that modulate heme peroxidase 2 gene involved in shell pigmentation. Several studies reported that there is a close relationship between shell formation and pigmentation (Nagai et al., 2007; Sun et al., 2015). In this study, three novel genes, *CgPOU2F1*, *CgSox5*, and *CgPax6* were identified. Expression analysis indicate that they were expressed in shell-field during shell formation.

The transcription factor POU2F1 is a member of the POU domain family ubiquitously expressed in both larval and adult tissues. POU2F1 has multiple functions in growth regulation and disease development (Zhang et al., 2013). It has been reported that POU2F1 drives miR-415a expression and promotes osteoblast differentiation (Xie et al., 2016). In *P. fucata*, POU2F1 has been implicated in activating *Aspein* gene to regulate shell formation (Gao et al., 2016). Data from in situ analysis showing the *CgPOU2F1* expression in the shell field area are consistent with its potential function in early shell plate morphogenesis and shell formation.

Sox gene family encodes a group of transcription factors containing the Sry-related HMG box domain. Sox genes play crucial roles in cell fate specification and differentiation (Kamachi and Kondoh, 2013). Among members of the Sox family, genetic studies demonstrated that knockouts *Sox5* or *Sox6* lead to skeletal abnormalities in mice (Smits et al., 2001). Consistent with a potential role of *CgSox5* in shell formation, we showed by WISH studies that *CgSox5* expression occurs earlier in larval development than *CgPOU2F1* and *CgPax6*, and its expression was detected in shell gland cells of the gastrula embryos. Studies on *Lymnaea stagnalis* have demonstrated that the first organic shell is secreted from shell gland cells (Hohagen and Jackson, 2013).

The highly conserved paired box (Pax) transcription factors are vital for cell fate specification and tissue differentiation in various bilaterians (Scherholz et al., 2017). A recent study in brachiopods suggested that the *Pax6* may act as a transcriptional regulator to control the segment polarity gene *engrailed* expression (Vellutini and Hejnol, 2016). We showed here that engrailed expression was located in the shell-forming region during mollusk shell formation (Jacobs et al., 2000; Baratte et al., 2007). *CgPax6* was first detected in the shell-forming region at the trochophore stage, which correlates with prodissoconch I formation. It is possible that *Pax6* regulates *engrailed* gene expression during shell formation, although the target genes have yet to be identified to provide a better mechanistic understanding of *Pax6* function in shell formation.

Conclusions: In this study, we characterized the shell formation during larval development in *C. gigas*. By using SEM and fluorescent staining, we characterized the dynamic process of shell morphogenesis from trochophore to eyespot larvae. We demonstrated that the shell field displayed a series of morphological changes as shell develops from prodissoconch I and II to teloconch shell. We found a close connection between organic matrix secretion and $CaCO_3$ deposition during early shell formation. To better understand the molecular regulation of shell morphogenesis, we isolated three key transcriptional factors, *CgPOU2F1*, *CgSox5*, and *CgPax6,* that have been implicated in shell formation and bone development. Expression analysis revealed a colocalized pattern of gene expression and developing shell field formation, indicating that they may play a potential role in the initiation of shell morphogenesis and formation.

Supplementary data to this article can be found online at https://doi.org/10.1016/j.cbpb.2022.110783.

Declaration of Competing Interest

The authors declare no conflicts of interest.

Acknowledgments

This work was supported by the Agriculture Research System of China Project (CARS-49), and Earmarked Fund for Agriculture Seed Improvement Project of Shandong Province (2020LZGC016).

References

Addadi, L., Joester, D., Nudelman, F., Weiner, S., 2006. Mollusk shell formation: a source of new concepts for understanding biomineralization processes. Chem. Eur. J. 12, 981–987.

Aranda-Burgos, J.A., Da Costa, F., Novoa, S., Ojea, J., Martinez-Patino, D., 2014. Embryonic and larval development of Ruditapes decussatus (Bivalvia: Veneridae): a study of the shell differentiation process. J. Molluscan Stud. 80, 8–16.

Baratte, S., Andouche, A., Bonnaud, L., 2007. Engrailed in cephalopods: a key gene related to the emergence of morphological novelties. Dev. Genes Evol. 217, 353–362.

Berland, S., Ma, Y.F., Marie, A., Andrieu, J.P., Bedouet, L., Feng, Q.L., 2013. Proteomic and profile analysis of the proteins laced with aragonite and vaterite in the freshwater mussel *Hyriopsis cumingii* shell biominerals. Protein Pept. Lett. 20, 1170–1180.

Che, L.M., Golubic, S., Le Campion-Alsumard, T., Payri, C., 2001. Developmental aspects of biomineralisation in the Polynesian pearl oyster Pinctada margaritifera var. cumingii. Oceanol. Acta 24, S37–S49.

Exelby, K., Herrera-Delgado, E., Perez, L.G., Briscoe, J., et al., 2021. Precision of tissue patterning is controlled by dynamical properties of gene regulatory networks. Development 148, dev197566.

Fang, D., Xu, G.R., Hu, Y.L., Pan, C., Xie, L.P., Zhang, R.Q., 2011. Identification of genes directly involved in shell formation and their functions in pearl oyster, *Pinctada fucata*. PLoS One 6, e21860.

Freeman, G., Lundelius, J.W., 1999. Changes in the timing of mantle formation and larval life history traits in linguliform and craniiform brachiopods. Lethaia 32, 197–217.

Gao, J., Chen, Y., Yang, Y., Liang, J., Xie, J., Liu, J., et al., 2016. The transcription factor Pf-POU3F4 regulates expression of the matrix protein genes *Aspein* and *Prismalin-14* in pearl oyster (*Pinctada fucata*). FEBS J. 283, 1962–1978.

Hohagen, J., Jackson, D.J., 2013. An ancient process in a modern mollusc: early development of the shell in *Lymnaea stagnalis*. BMC Dev. Biol. 13.

Hohagen, J., Herlitze, I., Jackson, D.J., 2015. An optimised whole mount in situ hybridisation protocol for the mollusc *Lymnaea stagnalis*. BMC Dev. Biol. 15.

Huan, P., Liu, G., Wang, H.X., Liu, B.Z., 2013. Identification of a tyrosinase gene potentially involved in early larval shell biogenesis of the Pacific oyster *Crassostrea gigas*. Dev. Genes Evol. 223, 389–394.

Huan, P., Wang, H.X., Liu, B.Z., 2016. Assessment of housekeeping genes as internal references in quantitative expression analysis during early development of oyster. Genes Genet. Syst. 91, 257–265.

Jackson, D.J., Degnan, B.M., 2016. The importance of evo-devo to an integrated understanding of molluscan biomineralisation. J. Struct. Biol. 196, 67–74.

Jackson, D.J., McDougall, C., Woodcroft, B., Moase, P., Rose, R.A., Kube, M., et al., 2010. Parallel evolution of nacre building gene sets in molluscs. Mol. Biol. Evol. 27, 591–608.

Jacobs, D.K., Wray, C.G., Wedeen, C.J., Kostriken, R., DeSalle, R., Staton, J.L., et al., 2000. Molluscan engrailed expression, serial organization, and shell evolution. Evol. Dev. 2, 340–347.

Kamachi, Y., Kondoh, H., 2013. Sox proteins: regulators of cell fate specification and differentiation. Development 140, 4129–4144.

Kapsenberg, L., Miglioli, A., Bitter, M.C., Tambutte, E., Dumollard, R., Gattuso, J.P., 2018. Ocean pH fluctuations affect mussel larvae at key developmental transitions. Proc. R. Soc. B 285, 20182381.

Lee, S.W., Hong, S.M., Choi, C.S., 2006. Characteristics of calcification process in embryos and larvae of the Pacific oyster, *Crassostrea gigas*. Bull. Mar. Sci. 78, 309–317.

Liao, Z., Bao, L.F., Fan, M.H., Gao, P., Wang, X.X., Qin, C.L., et al., 2015. In-depth proteomic analysis of nacre, prism, and myostracum of Mytilus shell. J. Proteome 122, 26–40.

Liu, G., Huan, P., Liu, B.Z., 2015. A GATA2/3 gene potentially involved in larval shell formation of the Pacific oyster *Crassostrea gigas*. Dev. Genes Evol. 225, 253–257.

Liu, G., Huan, P., Liu, B.Z., 2017. A SoxC gene related to larval shell development and co-expression analysis of different shell formation genes in early larvae of oyster. Dev. Genes Evol. 227, 181–188.

Marie, B., Marie, A., Jackson, D.J., Dubost, L., Degnan, B.M., Milet, C., et al., 2010. Proteomic analysis of the organic matrix of the abalone *Haliotis asinina* calcified shell. Proteome Sci. 8.

Marie, B., Zanella-Cleon, I., Guichard, N., Becchi, M., Marin, F., 2011. Novel proteins from the calcifying shell matrix of the Pacific oyster *Crassostrea gigas*. Mar. Biotechnol. 13, 1159–1168.

Marie, B., Jackson, D.J., Ramos-Silva, P., Zanella-Cleon, I., Guichard, N., Marin, F., 2013. The shell-forming proteome of *Lottia gigantea* reveals both deep conservations and lineage-specific novelties. FEBS J. 280, 214–232.

Marin, F., Amons, R., Guichard, N., Stigter, M., Hecker, A., Luquet, G., et al., 2005. Caspartin and calprismin, two proteins of the shell calcitic prisms of the Mediterranean fan mussel *Pinna nobilis*. J. Biol. Chem. 280, 33895–33908.

Miglioli, A., Dumollard, R., Balbi, T., Besnardeau, L., Canesi, L., 2019. Characterization of the main steps in first shell formation in *Mytilus galloprovincialis*: possible role of tyrosinase. Proc. R. Soc. B 286, 20192043.

Miyazaki, Y., Nishida, T., Aoki, H., Samata, T., 2010. Expression of genes responsible for biomineralization of *Pinctada fucata* during development. Comp. Biochem. Physiol. Part B Biochem. Mol. Biol. 155, 241–248.

Nagai, K., Yano, M., Morimoto, K., Miyamoto, H., 2007. Tyrosinase localization in mollusc shells. Comp. Biochem. Physiol., Part B: Biochem. Mol. Biol 146, 207–214.

Ramesh, K., Melzner, F., Griffith, A.W., Gobler, C.J., Rouger, C., Tasdemir, D., Nehrke, G., 2018. In vivo characterization of bivalve larval shells: a confocal Raman microscopy study. J. R. Soc. Interface 15, 20170723.

Rose, R.A., Baker, S.B., 1994. Larval and spat culture of the Western Australian sliver- or goldlip pear oyster, *Pinctada maxium* Jameson (Mollusca: Pteriidase). Aquaculture 126, 35–50.

Scherholz, M., Redl, E., Wollesen, T., de Oliveira, A.L., Todt, C., Wanninger, A., 2017. Ancestral and novel roles of Pax family genes in mollusks. BMC Evol. Biol. 17.

Smits, P., Li, P., Mandel, J., Zhang, Z.P., Deng, J.M., Behringer, R.R., de Crombrugghe, B., Lefebvre, V., 2001. The transcription factors L-sox5 and sox6 are essential for cartilage formation. Dev. Cell 1, 277–290.

Song, X.R., Liu, Z.Q., Wang, L.L., Song, L.S., 2019. Recent advances of shell matrix proteins and cellular orchestration in marine molluscan shell biomineralization. Front. Mar. Sci. 6.

Sun, X.J., Yang, A.G., Wu, B.A., Zhou, L.Q., Liu, Z.H., 2015. Characterization of the mantle transcriptome of yesso scallop (*Patinopecten yessoensis*): identification of genes potentially involved in biomineralization and pigmentation. PLoS One 10.

Suzuki, M., Saruwatari, K., Kogure, T., Yamamoto, Y., Nishimura, T., Kato, T., Nagasawa, H., 2009. An acidic matrix protein, Pif, is a key macromolecule for nacre formation. Science 325, 1388–1390.

Vellutini, B.C., Hejnol, A., 2016. Expression of segment polarity genes in brachiopods supports a non-segmental ancestral role of engrailed for bilaterians. Sci. Rep. 6, 32387.

Xie, C.H., Cao, Y.M., Huang, Y., Shi, Q.W., Guo, J.H., Fan, Z.W., et al., 2016. Long non-coding RNA TUG1 contributes to tumorigenesis of human osteosarcoma by sponging miR-9-5p and regulating POU2F1 expression. Tumor Biol. 37, 15031–15041.

Zhang, G.F., Fang, X.D., Guo, X.M., Li, L., Luo, R.B., Xu, F., et al., 2012. The oyster genome reveals stress adaptation and the complexity of shell formation. Nature 490, 49–54.

Zhang, X.M., Ma, Y.Z., Liu, X.Y., Zhou, Q., Wang, X.J., 2013. Evolutionary and functional analysis of the key pluripotency factor Oct4 and its family proteins. J. Genet. Genom. 40, 399–412.

Zhao, R., Takeuchi, T., Luo, Y.J., Ishikawa, A., Kobayashi, T., Koyanagi, R., et al., 2018. Dual gene repertoires for larval and adult shells reveal molecules essential for molluscan shell formation. Mol. Biol. Evol. 35, 2751–2761.